Proceedings of ASME 2018 37th International Conference on Ocean, Offshore and Arctic Engineering
OMAE 2018
June 17-22, 2017, Madrid, Spain

OMAE2018-78119

THE TRIPLESPAR CAMPAIGN: VALIDATION OF A REDUCED-ORDER SIMULATION MODEL FOR FLOATING WIND TURBINES

Frank Lemmer (né Sandner), Wei Yu and Po Wen Cheng
Stuttgart Wind Energy (SWE)
University of Stuttgart
70569 Stuttgart, Germany
Email: lemmer@ifb.uni-stuttgart.de

Antonio Pegalajar-Jurado, Michael Borg, Robert F. Mikkelsen and Henrik Bredmose
Department of Wind Energy
Technical University of Denmark (DTU)
2800 Kgs. Lyngby, Denmark

ABSTRACT

Different research groups have recently tested scaled floating offshore wind turbines including blade pitch control. A test conducted by the University of Stuttgart (Germany), DTU (Denmark) and CENER (Spain) at the Danish Hydraulic Institute (DHI) in 2016 successfully demonstrated a real-time blade pitch controller on the public 10 MW *TripleSpar semi-submersible concept at a scale of 1/60. In the presented work a reduced-order simulation model including control is compared against the model tests. The model has only five degrees of freedom and is formulated either in the time-domain or in the frequency-domain. In a first step the Morison drag coefficients are identified from decay tests as well as irregular wave cases. The identified drag coefficients depend clearly on the sea state, with the highest ones for the decay tests and small sea states. This is an important finding, for example for the design of a robust controller, which depends on the system damping. It is shown that the simplified model can well represent the dominant physical effects of the coupled system with a substantially reduced simulation time, compared to state-of-the-art models.*

INTRODUCTION

Experimental testing has become especially important for Floating Offshore Wind Turbines (FOWTs) due to the additional dynamics from the floating substructure, mooring lines and wave forces. In the first place, model tests had the objective to validate software tools in general. But when the technological development advanced with the first tests in a realistic environment, model tests also helped to reduce the risk associated with the deployment of a prototype. An overview on a large number of past test campaigns can be found in [1]. The experience of these experiments has shown that scaled testing of FOWTs is challenging due to the multidisciplinary environment with aerodynamics, hydrodynamics, structural dynamics and servo (wind turbine control system) dynamics. One part of the present test focused on the replacement of the rotor and aerodynamics through an actuator. With this Hardware-In-the-Loop (HiL) approach a fan at the tower-top produces the equivalent thrust force based on a real-time simulation model, see [2]. The other part, which is the focus of this paper, used a wind generator system in the basin and a re-designed rotor for low Reynolds numbers.

The objective of the present campaign by the University of Stuttgart (Germany), DTU (Denmark) and CENER (Spain) in 2016 was to test the INNWIND.EU public floater, [3] with the DTU 10 MW reference wind turbine (RWT), [4], including blade pitch control. First results have been published already in [5] and [6]. A study with the same wind turbine and a higher-fidelity model was shown in [7]. A common methodology in other FOWT experiments was to maintain the rotor speed through a servo, actuating the torque. However, this servo controller was usually tuned aggressively to keep the rotor speed almost constant, see e.g. [8]. The blade-pitch angle is then constant with this methodology.

Recently, a number of researchers has taken the step to include the control system in scaled model tests after a first attempt had been made for the Hywind concept, see [9]. Tests at the Marine Research Institute of the Netherlands (MARIN) with different PI-controllers were presented in [10], assessing the controller influence on the response. Another test in the same basin was presented in [11]. An H_∞ controller was experimentally studied by Osaka Prefecture University, Japan, see [12].

Floater concept

Within the project INNWIND.EU a platform design competition among the project partners resulted in three different concepts, described in [13]. For the one, whose design began at the University of Stuttgart, a detailed design was done by CENER and the National Technical University of Athens (NTUA) towards the end of the project, see [14]. The mooring system design was a joint work by the University of Stuttgart and DTU. The concept is described in [3], it is public and a FAST model can be downloaded[1]. Figure 1 shows a sketch of the scaled FOWT: It is a deep-drafted semi-submersible with the prospect of combining the advantages of a spar with those of a semi-submersible. Thus, the draft is, with less than 60 m, less than the one of typical spar platforms and still, the material cost is reduced through simple cylindrical shapes, which can be made out of concrete. The properties of the TripleSpar concept are summarized in Table 1.

FIGURE 1: Scaled model of INNWIND.EU TripleSpar concept with DTU10 MW wind turbine.

Scaling and test setup

The platform was built at the University of Stuttgart in a scale of $\lambda = 1/60$ and assembled with a turbine model of the DTU 10 MW RWT, built at DTU, see Figure 2. The scaling laws applied follow Froude-scaling, see e.g. [15] and [16] (specific to FOWTs). Keeping a constant Froude number $Fr = v/\sqrt{gD}$ with velocity v, gravity constant g and characteristic diameter D results in forces scaled with λ^3 and a frequency scaled with $\lambda^{-\frac{1}{2}}$. Thus, smaller simulation timesteps and a higher sampling rate for sensors, processors, communication interfaces, etc. are necessary in model scale. Important additional dimensional numbers are the Keulegan-Carpenter number KC and the Reynolds number Re. While KC, important for hydrodynamic forcing, is maintained for the scaled system, Re is not. A method to mitigate the resulting mismatch of aerodynamic forcing has been to re-design the rotor, such that it is specifically suitable for low Reynolds numbers. The first tests done in the FOWT community addressing the scaling of aerodynamic forces were the DeepCwind tests, [17] and [18]. A comparison of experimental results to different simulation methods in the ongoing OC5 project can be found in [19].

The properties of the components of the present test setup were verified and identified with different methods. For the rotor, a Blade Element Momentum Theory (BEM) model was set up with the polars calculated by DTU [7] and the torque and thrust for different Tip-Speed Ratios (TSR) compared to the measurements, as shown in [6]. The tower structural properties were determined for a fixed configuration already for a previous test by DTU, see [7]. For the present configuration, this value was updated through an impulse response measurement of the towertop on the floating platform. The mass properties of the platform were calculated in detail via a parametric CAD model with the trimmed and final ballast configuration.

A measurement of the wind field without the turbine was made with a hot wire on a pulley system, see [5]. Due to a misplaced fan on the top of the wind generator array a higher wind speed could be measured at lower levels, creating an inverse shear. This might have an effect on the presented results. The turbulence intensity was measured also in [5]. In the simulations, a constant, uniform wind speed was used. The optical motion tracking system was set to update the reference position every day to the actual position of the Center of Flotation (CF). The presented results, however, show the displacements with respect to the global coordinate system, fixed to the basin. The wave generator was calibrated with numerous wave gauges, see [5]. The

[1] http://www.ifb.uni-stuttgart.de/windenergie/downloads

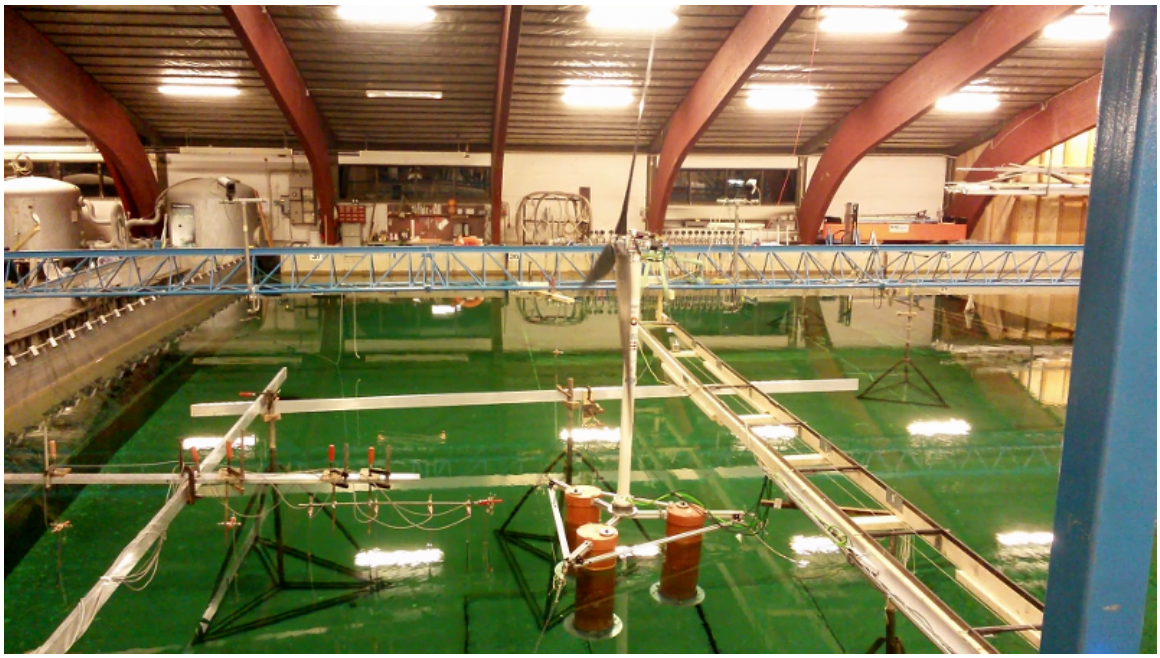

FIGURE 2: TripleSpar test setup at DHI 2016 in combined wind and wave tank.

highest uncertainty in the model parameters is likely the anchor position, also due to the high sensitivity of the mooring forces with respect to the position of the anchor. The wind generator produces an open jet, which implies an uncertainty about the velocity field in the rotor plane with blockage effects. This was studied in [20]. The hardware of the feedback controller including encoder and actuator has been thoroughly tested. However, the time lags or additional dynamics associated to the control system are not represented in the simulation model.

The environmental conditions for the test are shown in Table 2. Although a large range of sea states (and corresponding load cases (LCs)) has been defined only the higher-wave conditions are used in the following because of a limited response of the system to small waves. Due to splash water interruptions in the measured position signals occurred for LC 9. A large number of tests was performed also for regular waves, focused waves and misaligned waves. Therefore, the number of repetitions had to be limited in some cases.

REDUCED-ORDER SIMULATION MODEL

The employed model is based on a flexible multibody formulation with rigid and flexible bodies. The equations of motion are set up symbolically, depending on the definition of symbolic position vectors as a function of generalized coordinates, and exported to C for a fast model execution. In this work, the equations of motion have been set up for five DOFs in 2D: Four rigid DOFs as platform surge x_p, platform heave z_p, platform pitch β_p, rotor azimuth φ and the elastic tower-top fore-aft deformation x_{twr} giving the generalized coordinates

$$\mathbf{q} = [x_p,\, z_p,\, \beta_p,\, \varphi,\, x_{twr}]^T . \tag{1}$$

For a state-space description the state vector $\mathbf{x}$ results with the rotor speed Ω as

$$\mathbf{x} = \left[x_p,\, z_p,\, \beta_p,\, \varphi,\, x_{twr},\, \dot{x}_p,\, \dot{z}_p,\, \dot{\beta}_p,\, \Omega,\, \dot{x}_{twr}\right]^T . \tag{2}$$

These DOFs are selected in order to reduce the system to the most important dynamics, which are critical for conceptual design and control. Therefore, side-side dynamics (and every motion in lateral direction) are neglected, which is a consequence of the assumption that the design-driving loads act in the plane of the prevailing wind direction. The rigid bodies are the *platform*, *nacelle* and the *rotor* and the only elastic body is the *tower*. For a simplification of the tuning with the experiments the tower is modeled as a rigid body with a spring-damper coupling to the nacelle and not as a beam with distributed structural properties. The individual rotor blades are not included in this model but the rotor is modeled as a rigid disk. This method neglects the coupling of flapwise blade dynamics with the tower modes. These simplifications accelerate the model execution significantly and allow for a clear view on the main system dynamics.

Aerodynamic forces are calculated using the aerodynamic rotor coefficients, namely the power and thrust coefficient, which

	full scale	model scale
Platform draft [m]	54.5	0.9
Platform column diameter [m]	15.0	0.25
Platform column spacing (to centerline) [m]	26.0	0.43
Platform mass [kg]	2.8×10^7	127.4
Platform mass moment of inertia about hor. axis @SWL [kg m^2]	1.9×10^{10}	32.25
Platform added mass moment of inertia about hor. axis @SWL [kg m^2]	1.1×10^{10}	16.29
Number of mooring lines [-]	3	
Water depth [m]	180.0	3.0
Mooring line length [m]	610.0	9.95
Turbine mass [kg]	1.1×10^6	5.7
Rated rotor speed [rpm]	9.6	74.4
Rated wind speed [m/s]	11.4	1.5

TABLE 1: INNWIND.EU TripleSpar platform and DTU10 MW wind turbine full scale and model parameters.

TABLE 2: LCs defined for irregular wave tests.

	Model scale			Full scale		
LC	H_s [m]	T_p [s]	$\bar{v}$ [m/s]	H_s [m]	T_p [s]	$\bar{v}$ [m/s]
7	0.09	1.08	1.89	5.46	8.37	14.6
9	0.16	1.43	1.89	9.54	11.1	14.6

are generated using BEM theory for various TSR and blade pitch angles θ. The aerodynamic damping is accounted for by calculating the relative rotor-effective wind speed. The three catenary mooring lines are represented by a nonlinear quasi-static model, which is based on the mooring line formulation of FAST v7, see [21]. It gives, for each mooring line, the horizontal and vertical forces on the platform depending on its position. For the linearization a perturbation analysis is done at the respective operating point resulting in a 6×6 stiffness matrix.

First-order hydrodynamics include the panel code force transfer function and a simplification of the radiation problem: A constant added-mass is assumed in all considered directions, interpolated at the eigenfrequency of the respective DOF of the frequency-dependent panel code results. Further, there is no radiation damping included, neither in the time-domain, nor in the frequency-domain model. It was found that this simplification yields substantial advantages in terms of computational efficiency with small differences in the response, mainly in the frequency range of the waves, depending on the floater shape.

Second-order hydrodynamics were included to account for the large response at the floater eigenfrequencies, below the wave frequencies. The same behavior, with low-frequency resonances, was also found in previous studies, like [8]. The forces result from a quadratic potential flow model at the difference-frequency of a bi-chromatic wave train, see [22]. Newman's approximation [23] is used here, which allows an efficient calculation of the low-frequency forces. It requires only the mean drift coefficients, which are the diagonal of the quadratic transfer function (QTF). The forces result from a single inverse Fourier transform, instead of a double one for the full difference-frequency calculation.

The CPU time of the nonlinear model is $1/120$ of the simulated time on a 2.5 GHz processor and the frequency-domain model is even faster as it only needs matrix-algebraic operations. This number excludes the necessary pre-processing of the aerodynamic rotor coefficients, the hydrodynamic coefficients, the symbolic equations of motion (only once for the TripleSpar platform) and the wave forces (for each load case). More information on the model can be found in [24]. A comprehensive publication of the physical assumptions, experimental and code-to-code comparisons is under preparation.

TESTED CONTROLLER

The rotor speed controller used in the following tests was designed in [6], following a method proposed in [25]. The gain scheduling of the proportional gain k_p, shown in Figure 3, together with the steady-state blade pitch angles, Figure 4, ensures a stable system for all operating points with a fixed time constant $T_i = 2.9$ s for all wind speeds. This method accounts for the negative damping of FOWTs, due to the zero with positive real part in the dynamics from blade pitch angle θ to the rotor speed Ω. The shape of the gain scheduling function resembles the one of the corresponding full-scale controller, see [3] with decreasing values for wind speeds above rated and increasing values for higher wind speeds, close to cut-out. This is due to the fact that the system is more stable towards higher wind speeds and thus the controller can be tuned more aggressively towards cut-out.

MODEL VALIDATION

The first part of this section addresses the identification of the Morison drag coefficients C_D for the columns and $C_{D,hp}$ for

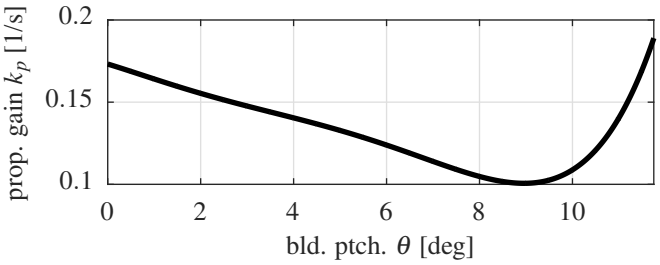

FIGURE 3: Proportional gains k_p over steady state blade pitch angles associated with time constant $T_i = 2.9\,\mathrm{s}$.

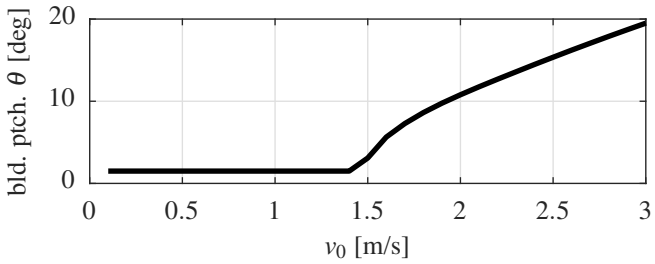

FIGURE 4: Steady state blade pitch angles θ over wind speeds v_0.

the heave plates with free-decay tests but also irregular wave cases with wind excitation and active blade pitch control. Thus, the hydrodynamic drag identification is in the latter case done with the full coupled system including aerodynamics. The second part of the section addresses additionally the rotor rotor speed and blade pitch angle with a comparison of the nonlinear time-domain model against the linear frequency-domain model.

TABLE 3: Coupled system eigenfrequencies.

DOF	Surge	Heave	Pitch	Tower
Eigenfrequency [Hz]	0.05	0.469	0.275	3.23

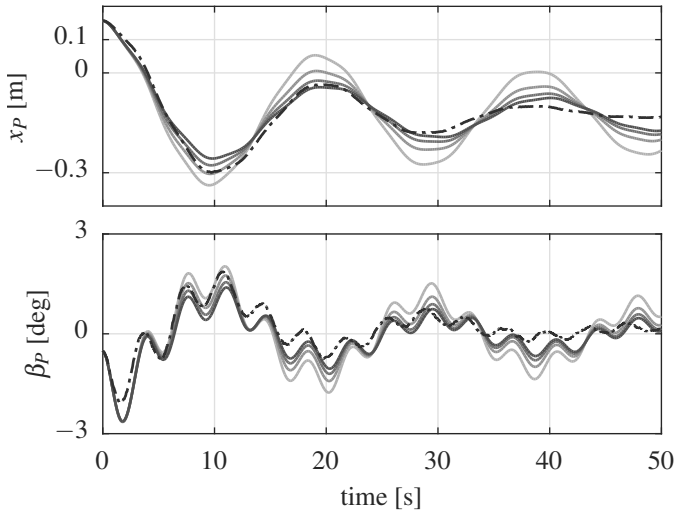

(a) Surge: Morison drag $C_D = [0.5, 1.0, 1.5, 2.0]$ (increasing darkness), $C_{D,hp} = 25$

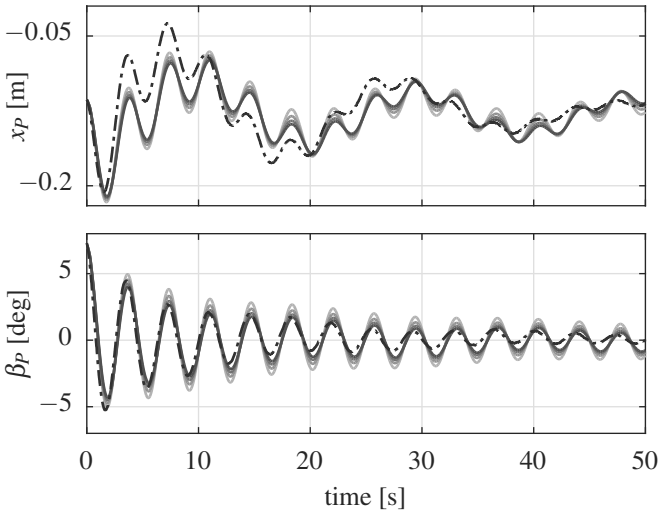

(b) Pitch: Morison drag $C_D = [2.0]$, $C_{D,hp} = [10, 15, 20, 25]$ (increasing darkness)

FIGURE 5: Free decay in surge and pitch directions and experiment (dashed line).

Hydrodynamic drag identification

Several methods to identify both Morison coefficients C_D and C_A are proposed in [15, p. 12-9]. However, these are particularly adapted to the times of little computational resources when full simulations of the experiments where not yet possible. Here we focus on the drag identification (C_D) and rely on the added mass computed by the panel code. A thorough tuning for a low-drafted semi-submersible for a FOWT was presented in [26]. Here, we will in a first step analyze free decay tests in surge x_p and pitch β_p. The drag coefficients resulting from such a free-decay identification were used in the OC5 phase II study [27] for all load cases. In this work, the drag is identified for each load case individually, which is justified through the varying *Re* and *KC* numbers, depending on the environmental conditions and the system response. With irregular waves the Morison coefficient C_D (columns) influences most the surge response while $C_{D,hp}$ (heave plates) influences more the heave

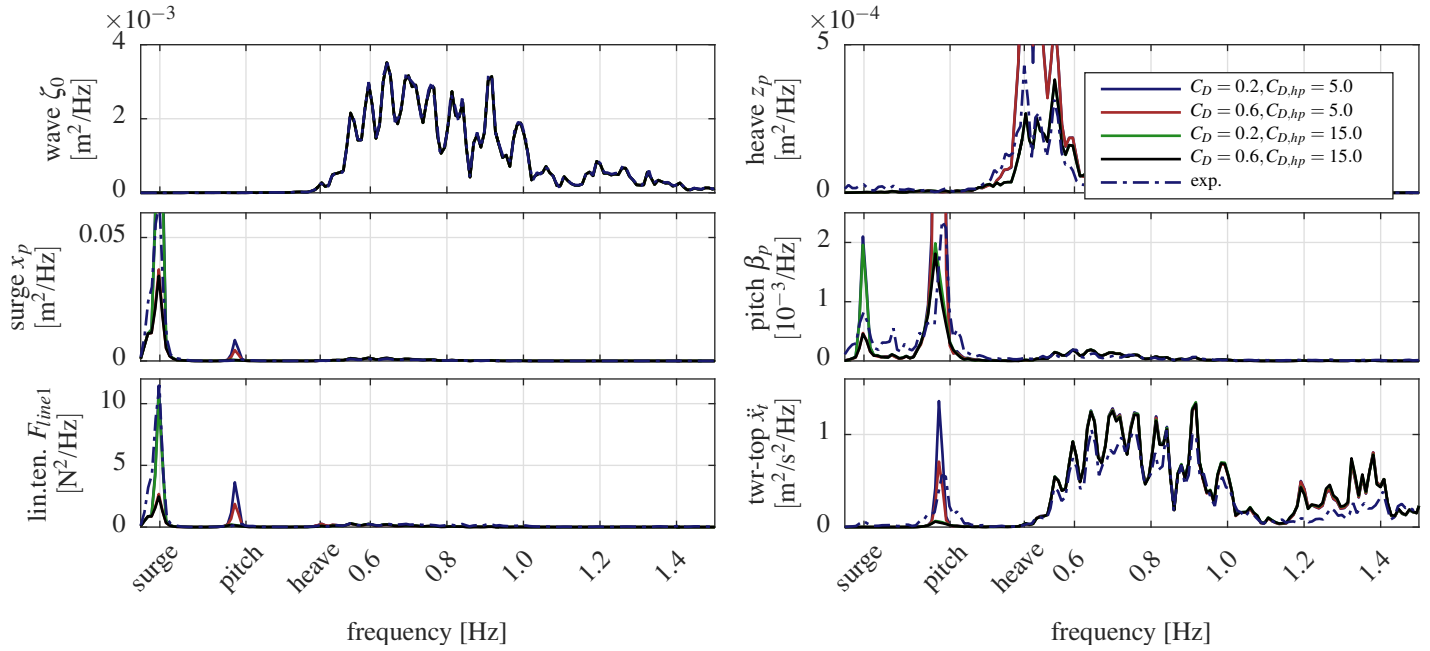

FIGURE 6: Response to wind and waves, LC 9 (Table 2) with simulations of various combinations of C_D and $C_{D,hp}$ and experiment (dashed). See following graphs for detailed views.

and pitch response. Figure 5 shows simulations of various C_D for the surge-decay on top and of various $C_{D,hp}$ for the pitch-decay below. The best agreement for both cases is with $C_D = 2.0$ and $C_{D,hp} = 25.0$.

In a next step, the drag is identified in irregular wave tests: Figure 6 shows the power spectral density (PSD) of the measured and simulated response for different combinations of both, the Morison drag coefficient C_D of the TripleSpar columns and the heave plate drag $C_{D,hp}$ for LC 9. The shown sensors are the wave height ζ_0, the platform heave z_p, surge x_p and pitch β_p and the upwind mooring line force F_{line1} (to the right looking upwind, at 60 deg) and tower-top acceleration $\ddot{x}_t$. Note that $\ddot{x}_t$ is the acceleration measured by the accelerometer and thus in the inertial frame, not relative to the tower base, as x_{twr} of Eq. 2. Therefore, $\ddot{x}_t$ is obtained from the simulation model through a transformation of $\dot{\mathbf{x}}$. On top of Figure 6 the peak spectral wave frequency at around 0.8 Hz is clearly visible. In this range the platform damping is of no effect as the waves yield a forced response at frequencies distant from the system eigenfrequencies. The velocity-dependent Morison excitation force term, however, can be of importance for platforms with larger KC numbers (e.g. smaller diameters). This was shown for the drag tuning in [26]. Here, the inertia forces of Morison's equation showed to be dominant with little velocity-dependent excitation.

At the wave frequencies the response magnitude in surge and pitch is small, for measurements and simulations. A greater response can be seen for platform-DOFs below the wave frequencies, at the platform surge, heave and pitch eigenfrequencies, listed in Table 3. At these frequencies, the wave height spectrum (ζ_0) is zero, so the excitation results from either second-order slow drift loads, as introduced in the modeling section, or the aerodynamic excitation. In a previous study [8], it was found that the contribution from the difference-frequency forcing is dominant over the one from aerodynamic forcing. It can be seen in Figure 6 that the response magnitudes at the eigenfrequencies depend significantly on the Morison drag coefficients (different colors).

Therefore, the focus will be on the frequency range below the wave spectrum for the identification of the Morison drag coefficients. In the following the irregular wave and wind response to the severest conditions, LC 9, will be shown. Figure 7 shows the variation of C_D while Figure 8 shows the corresponding variation of $C_{D,hp}$ with constant C_D. From Figure 7 it can be seen that the surge response for $C_D = 0.4$ gives the best agreement with the measurements. Since for FOWTs the heave response is not as important as the pitch response, the focus is put on the pitch-direction. With a heave plate drag of $C_{D,hp} = 10$ the best agreement with the pitch-response (β_p) can be achieved.

The simulated response of the tower at the pitch eigenfrequency does not match as well as for the wave response. As mentioned above, a main difference between the two response peaks is that for the surge and pitch resonances damping is important, while it is not for the wave response. Consequently, a difference in the aerodynamic damping or the tower structural

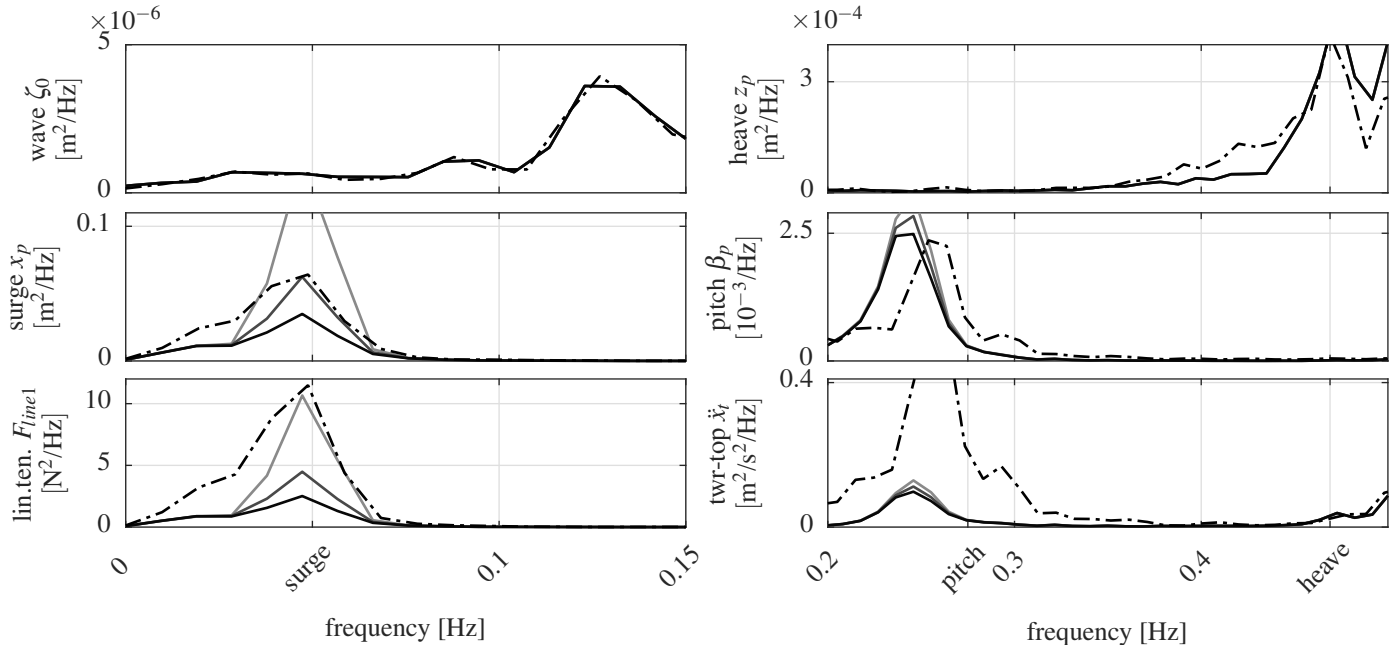

FIGURE 7: Response to wind and waves, LC 9 (Table 2) with simulations of Morison drag $C_D = [0.2, 0.4, 0.6]$ (increasing darkness), $C_{D,hp} = 10$ and experiment (dashed line).

damping could lead to the underpredicted surge and pitch resonance. It is noted that, although the eigenmode is labeled "pitch" in Table 3, this mode does also include a response of the tower-DOF x_{twr}. The mooring line force is always underpredicted by the model in the resonance frequencies (surge and pitch) but also in the wave frequency range. The reason for this is possibly the quasi-static modeling approach. If a mooring line mode lies close to the platform resonances the dynamic forces can be significantly higher, see also [19]. Works are ongoing related to the sensitivity of the results on the mooring line model fidelity.

A remarkable effect is that the pitch eigenfrequency changes compared to the free-decay test. The x-axis labels in Figure 8 correspond to the pitch eigenfrequency of the decay test, Figure 5. In Figures 7–8 both, the simulated and measured response have a lower pitch resonance, although the simulated response is slightly smaller than the measured one. This is due to the coupling with the controller dynamics, which were not active in the free-decay test.

The different drag values C_D and $C_{D,hp}$, were so far identified for decay tests and LC 9. The collection of drag coefficients in Table 4 includes also the less severe irregular wave test of LC 7. It can be seen that the drag is highest for the decay tests and decreases with the severity of the sea state or the magnitude of the response. It suggests that it is difficult to identify drag coefficients in general. As the drag depends strongly on the state of the flow surrounding the members a LC-dependent drag is necessary. This is in line with the findings of [26], who could well identify the drag for irregular sea states but found a mismatch of the simulation results when applying the obtained drag to wind-only cases.

The drag coefficients of Table 4 were compared with literature data: In [28] experimentally determined drag coefficients for thin heave plates are given as a function of KC. The values for $C_{D,hp}$, as well as their trend over KC, is close to the values of Table 4. The column drag of $C_D = 0.4$ is below the one defined in [29] for smooth cylinders.

TABLE 4: Identified Morison drag coefficients.

Load case	Morison drag C_D	Heave plate drag $C_{D,hp}$
Free decay	2.0	25.0
LC 7	0.6	20.0
LC 9	0.4	10.0

With the obtained drag coefficients and a reasonable agreement of the platform signals the full system response including the rotor signals will be compared to the nonlinear and the linearized simulation model.

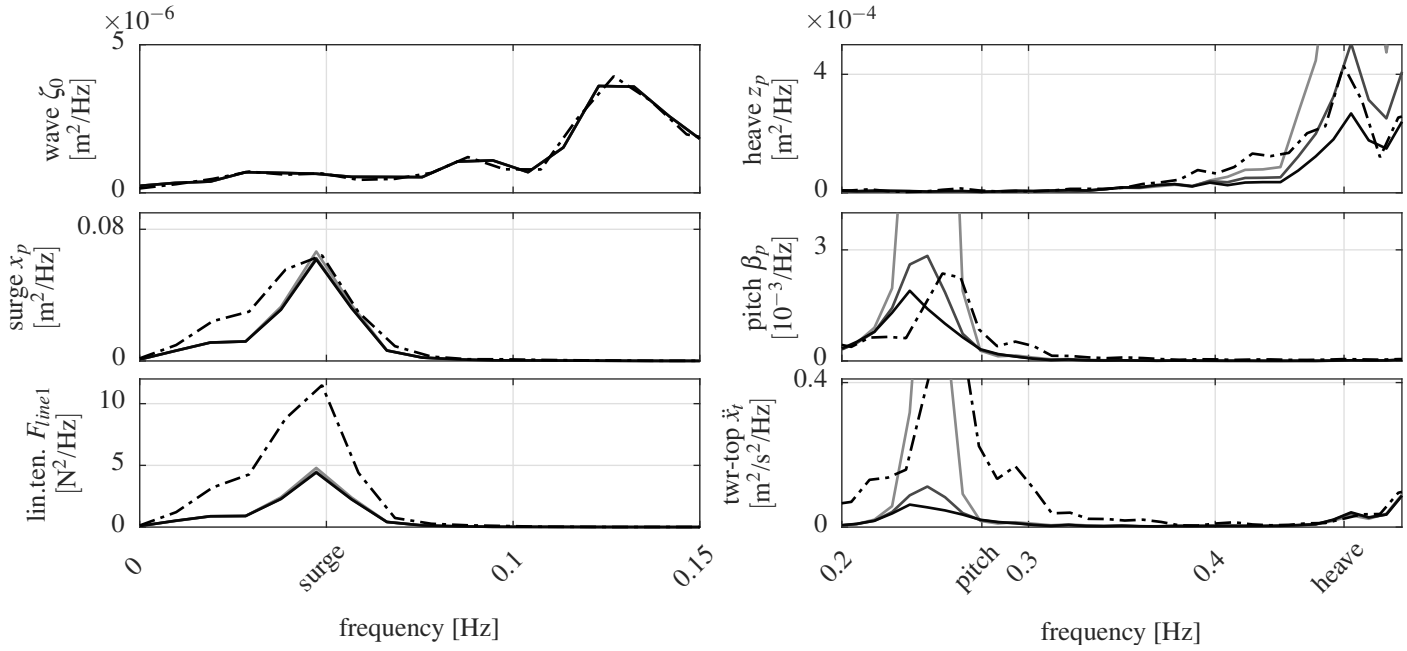

FIGURE 8: Response to wind and waves, LC 9 (Table 2) with simulations of Morison drag $C_D = 0.4$, $C_{D,hp} = [5, 10, 15]$ (increasing darkness) and experiment (dashed line).

Full system response

The previous section addressed already results of the full operating, blade-pitch controlled FOWT with wind and wave excitation. In this section, a comparison between the nonlinear and the linear simulation model in the less severe LC 7 is shown. Figure 9 shows the response of the rotor speed signal Ω and the blade pitch angle θ of the nonlinear and the linearized model. The frequency-domain model agrees very well with the nonlinear model suggesting that the response is still in the linear range in these environmental conditions. The agreement is equally good in the more severe LC 9 (not shown). The fact that the simplified simulation models can predict the main system characteristics of the FOWT confirms that few physical effects drive the dynamic response, while several others can be neglected in many states of operation and environmental loading conditions. One effect, which drives the computational efficiency is the radiation memory effect. It is neglected in both, the frequency-domain and the time-domain model with a zero radiation damping and a frequency-independent added mass, interpolated at the eigenfrequencies.

For the previously analyzed signals surge, heave and pitch, the agreement is good, also at the smaller magnitudes, visible in the logarithmic y-scale. The rotor speed and blade pitch signal is underpredicted by the simulation models at the wave frequencies. The reason for this is not known exactly. Two possible reasons are the wind and the aerodynamic simulation model and the drivetrain model. In this work, the wind is assumed to be constant and without shear. Thus, no turbulence and azimuth-dependent forcing is considered. In the experiment, the generated wind field could lead to an additional excitation, not represented in the simulation model. The aerodynamic forces, based on the wind signal, are assumed to be quasi-static. Research on unsteady aerodynamics for FOWTs was recently presented in [30], suggesting a necessary refinement of the aerodynamic model. As another possible explanation the drivetrain could have a combination of static and viscous friction and damping, which is not represented in the numerical model. This could yield a larger response of the rotor to wave-induced hub motion in the tests.

CONCLUSIONS

A reduced-order model was compared to wind-and-wave tank experiments of a floating offshore wind turbine model in a scale of $1/60$. As a first step, the experimental data was used to tune the drag coefficients for the three vertical columns of the TripleSpar floater, as well as for the heave plates at their lower ends. The drag identification showed an important dependence of the hydrodynamic drag coefficients on the response magnitude. Due to the strong coupling of the platform pitch mode and the rotor mode, this damping is important for the prediction of load and motion response ranges but also for a robust tuning of the wind turbine controller. The reduced-order model in the time-domain as well as in the frequency-domain formulation can model the main dynamics seen in the experiments. The response to irre-

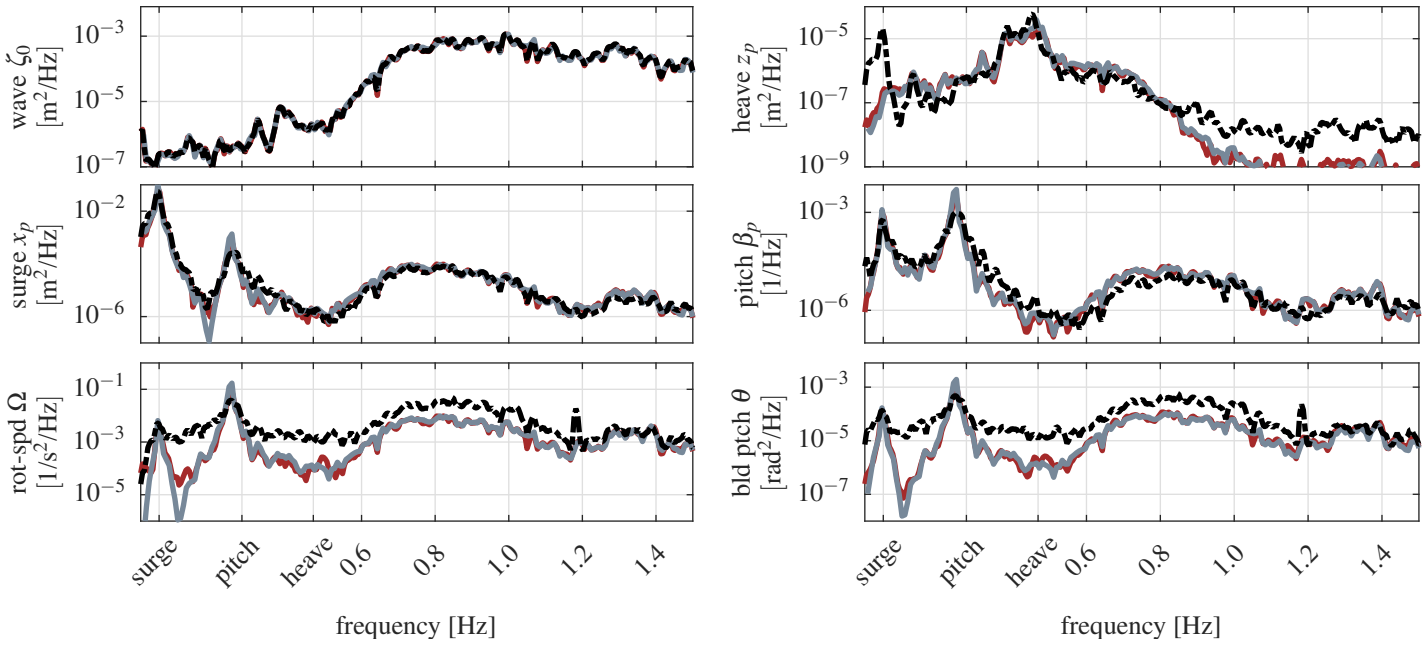

FIGURE 9: Response to wind and waves, LC 7 (Table 2) with nonlinear model (red) and linear model frequency-domain model (grey); note log-scale on *y*-axis.

gular waves and wind including the feedback controller agrees well in terms of magnitude, but also in terms of eigenfrequencies. Especially for the platform states, the model fidelity proves to be sufficient to reliably predict the motion response in terms of the PSD.

Differences between model and measurements are present for the tower-top acceleration, the mooring line force and the rotor speed and the blade-pitch response. Here, the main reasons are expected to be uncertain model parameters like the anchor position, the tower mass, stiffness and damping distribution (including electrical cables). For the rotor speed and blade pitch angle, the wind and aerodynamic model should be refined. Also, a detailed identification of the drivetrain friction should be considered in future works. The uncertainty of the model parameters and the wind field has not been quantified in this study. These are necessary steps for future test campaigns.

ACKNOWLEDGMENT

The presented research results from a joint project between DTU, CENER and the University of Stuttgart, based on previous works supported by the EU Seventh Framework Program (FP7) under grant no. 308974 (INNWIND.EU). The support from DHI is greatly acknowledged. The analysis of the results has received funding from the European Union's Horizon 2020 research and innovation programme under grant no. 640741 (LIFES50+).

REFERENCES

[1] Müller, K., Sandner, F., Bredmose, H., Azcona, J., Manjock, A., and Pereira, R., 2014. "Improved tank test procedures for scaled floating offshore wind turbines". In International Wind Engineering Conference IWEC.

[2] Vittori, F., Bouchotrouch, F., Lemmer, F., and Azcona, J., 2018. "Hybrid scaled testing of a 5MW floating wind turbine using the SIL method compared with numerical models". In Proceedings of the ASME 37th International Conference on Ocean, Offshore and Arctic Engineering.

[3] Lemmer, F., Amann, F., Raach, S., and Schlipf, D., 2016. Definition of the SWE-TripleSpar floating platform for the DTU 10MW reference wind turbine. Tech. rep., University of Stuttgart.

[4] Bak, C., Zahle, F., Bitsche, R., Kim, T., Yde, A., Henriksen, L., Natarajan, A., and Hansen, M., 2013. Description of the DTU 10MW reference wind turbine. Tech. rep., Technical University of Denmark, Roskilde, Denmark.

[5] Bredmose, H., Lemmer, F., Borg, M., Pegalajar-Jurado, A., Mikkelsen, R. F., Stoklund Larsen, T., Fjelstrup, T., Yu, W., Lomholt, A. K., Boehm, L., and Azcona, J., 2017. "The TripleSpar campaign: Model tests of a 10MW floating wind turbine with waves, wind and pitch control". *Energy Procedia,* ***137***, pp. 58–76.

[6] Yu, W., Lemmer, F., Bredmose, H., Borg, M., Pegalajar-Jurado, A., Mikkelsen, R. F., Stoklund Larsen, T., Fjelstrup, T., Lomholt, A., Boehm, L., Schlipf, D., and Azcona, J.,

2017. "The TripleSpar Campaign: Implementation and test of a blade pitch controller on a scaled floating wind turbine model". In Energy Procedia, Vol. 137, Elsevier, pp. 323–338.

[7] Pegalajar-Jurado, A., Hansen, A. M., Laugesen, R., Mikkelsen, R. F., Borg, M., Kim, T., Heilskov, N. F., and Bredmose, H., 2016. "Experimental and numerical study of a 10MW TLP wind turbine in waves and wind". *Journal of Physics: Conference Series,* ***753***.

[8] Borisade, F., Koch, C., Lemmer, F., Cheng, P. W., and Matha, D., 2017. "Validation of INNWIND.EU scaled model tests of a semisubmersible floating wind turbine". *International Journal of Offshore and Polar Engineering,* ***28***(1), pp. 54–64.

[9] Skaare, B., Hanson, T. D., Nielsen, F. G., Yttervik, R., Hansen, A. M., Thomsen, K., and Larsen, T. J., 2007. "Integrated dynamic analysis of floating offshore wind turbines". In Proceedings of the European Wind Energy Conference.

[10] Goupee, A. J., Kimball, R. W., and Dagher, H. J., 2017. "Experimental observations of active blade pitch and generator control influence on floating wind turbine response". *Renewable Energy,* ***104***, pp. 9–19.

[11] Savenije, F., 2017. "Model testing of a floating wind turbine including control". In EERA Deepwind.

[12] Hara, N., Tsujimoto, S., Nihei, Y., Iijima, K., and Konishi, K., 2017. "Experimental validation of model-based blade pitch controller design for floating wind turbines: System identification approach". *Wind Energy,* ***20***(7), pp. 1187–1206.

[13] Sandner, F., Yu, W., Matha, D., Azcona, J., Munduate, X., Grela, E., Voutsinas, S., and Natarajan, A., 2014. INNWIND.EU D4.33: Innovative concepts for floating structures. Tech. rep., University of Stuttgart.

[14] Azcona, J., Palacio, D., Munduate, X., González, L., and Nygaard, T. A., 2016. "Impact of mooring lines dynamics on the fatigue and ultimate loads of three offshore floating wind turbines computed with IEC 61400-3 guideline". *Wind Energy,* ***20***(5), pp. 797–813.

[15] Journée, J., and Massie, W. W., 2001. *Offshore Hydromechanics*, 1st ed. Delft University of Technology.

[16] Bredmose, H., Larsen, S. E., Matha, D., Rettenmeier, A., Marino, E., and Saettran, L., 2012. MARINET D2.4: Collation of offshore wind-wave dynamics. Tech. rep., Technical University of Denmark.

[17] Goupee, A., Koo, B., Lambrakos, K., and Kimball, R., 2012. "Model tests for three floating wind turbine concepts". In Proceedings of the Offshore Technology Conference.

[18] Robertson, A., Goupee, A., Jonkman, J., Prowell, I., Molta, P., Coulling, A., and Masciola, M., 2013. "Summary of conclusions and recommendations drawn from the DeepCwind scaled floating offshore wind system test campaign". In Proceedings of the ASME 32nd International Conference on Ocean, Offshore and Arctic Engineering.

[19] Robertson, A., Wendt, F., Jonkman, J. M., Popko, W., Dagher, H. J., Gueydon, S., Qvist, J., Vittori, F., Azcona, J., Uzunoglu, E., Soares, C. G., Harries, R., Yde, A., Galinos, C., Hermans, K., de Vaal, B. J., Bozonnet, P., Bouy, L., Bayati, I., Bergua, R., Galvan, J., Mendikoa, I., Barrera, C., Shin, H., Oh, S., Molins, C., and Debruyne, Y., 2017. "OC5 project phase II: Validation of global loads of the DeepCwind floating semisubmersible wind turbine". *Energy Procedia,* ***137***, pp. 38–57.

[20] Klein, L., Schulz, C., Lutz, T., and Krämer, E., 2016. "Influence of jet flow on the Aerodynamics of a floating model wind turbine". In Proceedings of the 26th International Ocean and Polar Engineering Conference, pp. 403–410.

[21] Jonkman, J., and Buhl, M., 2005. FAST user's guide. Tech. rep., National Renewable Energy Laboratory, Boulder, USA.

[22] Faltinsen, O. M., 1993. *Sea Loads On Ships And Offshore Structures*. Cambridge University Press.

[23] Standing, R., Brendling, W., and Wilson, D., 1987. "Recent developments in the analysis of wave drift forces, low-frequency damping and response". In Proceedings of the Offshore Technology Conference.

[24] Lemmer, F., Raach, S., Schlipf, D., and Cheng, P. W., 2016. "Parametric wave excitation model for floating wind turbines". *Energy Procedia,* ***94***, pp. 290–305.

[25] Sandner, F., Schlipf, D., Matha, D., and Cheng, P. W., 2014. "Integrated optimization of floating wind turbine systems". In Proceedings of the ASME 33rd International Conference on Ocean, Offshore and Arctic Engineering.

[26] Berthelsen, P. A., Bachynski, E., Karimirad, M., and Thys, M., 2016. "Real-time hybrid model tests of a braceless semi-submersible wind turbine. part III: Calibration of a numerical model". In Proceedings of the ASME 35th International Conference on Ocean, Offshore and Arctic Engineering.

[27] Robertson, A., 2017. "Uncertainty analysis of OC5-DeepCwind floating semisubmersible offshore wind test campaign". In Proceedings of the 27th International Ocean and Polar Engineering Conference, pp. 482–489.

[28] Tao, L., and Dray, D., 2008. "Hydrodynamic performance of solid and porous heave plates". *Ocean Engineering,* ***35***(10), pp. 1006–1014.

[29] DNV, 2007. DNV-RP-C205: Environmental conditions and environmental loads.

[30] Bayati, I., Belloli, M., Bernini, L., and Zasso, A., 2017. "A formulation for the unsteady aerodynamics of floating wind turbines, with focus on the global system dynamics". In Proceedings of the ASME 36th International Conference on Ocean, Offshore and Arctic Engineering.